Wenhui Niu, Yubin Fu, Hartmut Komber, Ji Ma, Xinliang Feng, Yiyong Mai, Junzhi Liu

Sulfur-Doped Nanographenes Containing Multiple Subhelicenes

Erstveröffentlichung in / First published in:

Organic Letters. 2021, 23 (6), S. 2069–2073. ACS Publications. ISSN 1523-7052.

DOI: https://doi.org/10.1021/acs.orglett.1c00232

Final edited form was published in "Organic Letters". 2021, 23 (6), S. 2069–2073. ISSN 1523-7052.
https://doi.org/10.1021/acs.orglett.1c00232

Sulfur-doped Nanographenes Containing Multiple Subhelicenes

Wenhui Niu[†‡], Yubin Fu[‡], Hartmut Komber[§], Ji Ma[‡], Xinliang Feng[‡], Yiyong Mai*[, †] and Junzhi Liu*[, #]

[†]School of Chemistry and Chemical Engineering, Frontiers Science Center for Transformative Molecules, Shanghai Key Laboratory of Electrical Insulation and Thermal Ageing, Shanghai Jiao Tong University, Shanghai 200240, China

[‡]Center for Advancing Electronics Dresden (cfaed) and Faculty of Chemistry and Food Chemistry, Technische Universität Dresden, D-01062 Dresden, Germany

[§]Leibniz-Institut für Polymerforschung Dresden e. V., D-01069 Dresden, Germany

[#]Department of Chemistry and State Key Laboratory of Synthetic Chemistry, The University of Hong Kong, Hong Kong 999077, China

ABSTRACT: In this work, we describe the synthesis and characterization of three novel sulfur-doped nanographenes (NGs) (**1**, **2** and **3**) containing multiple subhelicenes, including carbo[4]helicenes, thieno[4]helicenes, carbo[5]helicenes and thieno[5]helicenes. DFT calculations reveal that the helicene substructures in **1**-**3** possess dihedral angles from 15° to 34°. The optical energy gaps of **1**-**3** are estimated to be 2.67, 2.45 and 2.30 eV, respectively. These three sulfur-doped NGs show enlarged energy gaps compared to their pristine carbon analogues.

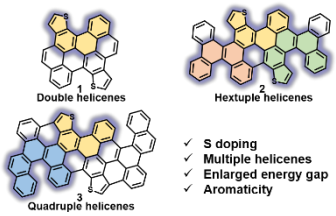

As an important class of nanographenes (NGs), nonplanar NGs adopt curved structures either by embedding nonhexagonal rings[1, 2] or by introducing steric strain from atom crowding[3], such as [4]helicene (cove-edged structure), [5]helicene (fjord-edged structure), and even higher helicenes[4-6]. Benefiting from the curvature, nonplanar NGs bearing helical substructures exhibit enhanced solubility compared to their planar counterparts, which enable the promising applications in organic field-effect transistors (OFETs)[3], chiral-induced spin selectivity[7], molecular recognition and machines, etc[8-10]. Apart from a number of examples of nonplanar NGs containing single helicene substructure[11-15], considerable progress has been made in multiple subhelicenes, which showed highly distorted geometry by accumulation of helical repulsion, as exemplified by **A**-**C**[16-18](Figure 1a). By the incorporation of multiple helicene substructures, those nonplanar NGs may not only exhibit richer three-dimensional geometry, more possible diastereomers and dynamics of isomerization, but also display unique molecular packing motifs[19,20], which favor their charge carrier transport in electronic devices[3].

Compared to their pristine carbon analogues, NGs doped with heteroatoms such as nitrogen, sulfur, boron in the aromatic skeleton have been shown to exhibit tailored optoelectronic properties[21-25]. Among them, sulfur-doped NGs have attracted growing interest in the past decade[26-28], due to their highly localized electronic structures contributed by the electron richness and polarizability of sulfur atoms. However, the sulfur-doped NGs with multiple subhelicenes have received limited attention[28, 29], mostly due to the lack of efficient synthetic strategies.

In this work, we report an efficient synthetic strategy towards three unprecedented sulfur-doped NGs containing two (**1**), six (**2**) and four (**3**) helicene substructures based on the well-controlled cyclodehydrogenation reactions (Figure 1b). Compound **1** consists of a pair of thieno[4]helicenes (yellow). Further lateral extension of **1** by fusing two phenanthrene units, compound **2** bearing additional two pairs of carbo[4]helicenes (orange) and thieno[5]helicenes (green) was achieved. Compound **3** containing an extra pair of carbo[5]helicenes (blue) was subsequently synthesized by fusing two chrysene moieties into **1**. Density functional theory (DFT) calculations revealed that the helicene substructures in **1**-**3** possess dihedral angles from 15° to 34°, which are responsible for the excellent solubility of these NGs. The aromaticity of the resultant NGs was evaluated to be aromatic character by calculations. This study opens a new avenue for the precise synthesis of novel nonplanar NGs, and also offers a new insight into the contributions of sulfur doping and helicene substructures to the physiochemical properties of NGs.

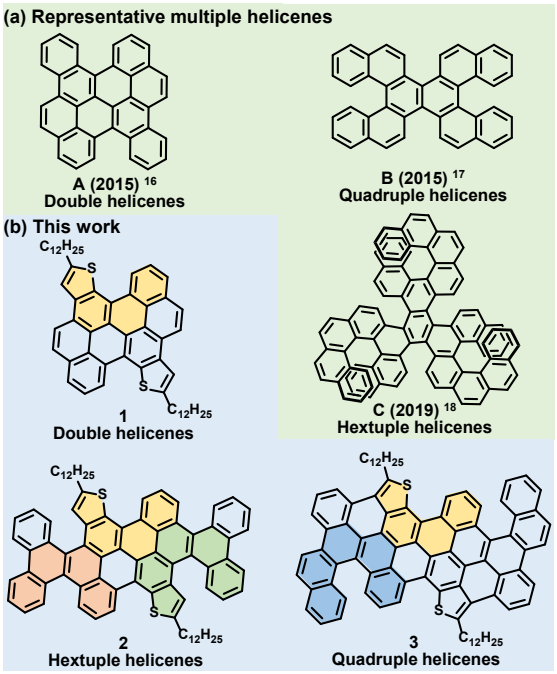

FIGURE 1. Structures of a) representative multiple helicenes and b) sulfur-doped NGs (**1**, **2** and **3**) with multiple helicene substructures reported in this work, including carbo[4]helicenes (orange), thieno[4]helicenes (yellow), carbo[5]helicenes (blue) and thieno[5]helicenes (green).

SCHEME 1. Schematic illustration of the synthesis of key building block 4.

Final edited form was published in "Organic Letters". 2021, 23 (6), S. 2069–2073. ISSN 1523-7052.
https://doi.org/10.1021/acs.orglett.1c00232

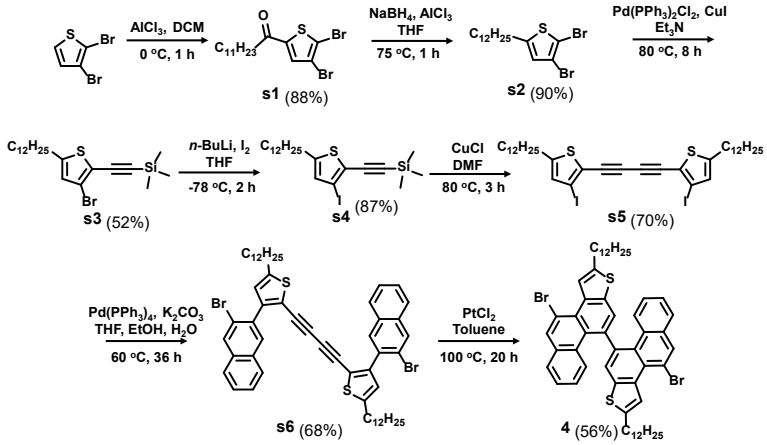

The synthetic routes toward **1**-**3** are illustrated in Scheme 1 and 2. First, the key building block 4,4'-dibromo-2,2'-didodecyl-10,10'-biphenanthro[2,1-*b*]thiophene (**4**) was synthesized as depicted in Scheme 1. Compound 2,3-dibromo-5-dodecylthiophene (**s2**) was obtained by Friedel-Crafts acylation reaction and carbonyl reduction in 88% and 90% yield, respectively. Afterward, a selective Sonogashira reaction of **s2** with trimethylsilylacetylene offered ((3-bromo-5-dodecylthiophen-2-yl)ethynyl)trimethylsilane (**s3**) in 52% yield. Then, the bromo groups were transformed into iodo groups, affording ((5-dodecyl-3-iodothiophen-2-yl)ethynyl)trimethylsilane (**s4**) in 87% yield. Glaser self-coupling of **s4** provided 1,4-bis(5-dodecyl-3-iodothiophen-2-yl)buta-1,3-diyne (**s5**) in 70% yield. Subsequently, 1,4-bis(3-(3-bromonaphthalen-2-yl)-5-dodecylthiophen-2-yl)buta-1,3-diyne (**s6**) was furnished through the Suzuki coupling of **s5** and 2-bromo-3-naphthaleneboronic acid in 68% yield. Then the Pt-induced cyclization of **s6** afforded compound **4** in 56% yield (see details in Supporting Information, SI).

The key intermediate compound **4** was subsequently subjected to the synthesis of precursor compounds for the final sulfur-doped NGs (Scheme 2). Treatment of **4** with *n*-butyllithium gave 2,2'-didodecyl-10,10'-biphenanthro[2,1-*b*]thiophene (**5**) in 92% yield. The two-fold Suzuki coupling of **4** afforded 4,4'-di([1,1'-biphenyl]-2-yl)-2,2'-didodecyl-10,10'-biphenanthro[2,1-*b*]thiophene (**6**) and 2,2'-didodecyl-4,4'-bis(2-(naphthalen-2-yl)phenyl)-10,10'-biphenanthro[2,1-*b*]thiophene (**7**) in 88% and 79% yield, respectively (Scheme 2). Finally, the well-controlled Scholl reactions allowed the formation of **1**-**3** containing multiple subhelicenes with good yields, including double, hextuple and quadruple helicenes, respectively (Scheme 2). Compound **1** was achieved from **5** in 89% yield by fusing two C-C bonds, leading to the formation of a pair of thieno[4]helicenes. Compound **2** was synthesized from **6** in 78% yield via the cyclization of four C-C bonds, resulting in two additional pairs of carbo[4]helicenes and thieno[5]helicenes. Compound **3** was obtained from **7** in 52% yield, in which six C-C bonds were fused and an extra pair of carbo[5]helicenes was generated accordingly. Interestingly, compound **3** fused two more C-C bonds than **2** during the cyclodehydrogenation. This is likely due to the different distance between the thiophene ring and opposite benzene ring in their precursors **6** and **7**, which is driven by their respective steric hindrance. All targeted compounds **1**-**3** were purified by preparative thin-layer chromatography, then recrystallized from dichloromethane (DCM) and methanol. The chemical identities of the targeted compounds **1**-**3** were confirmed by ^{1}H- and ^{13}C-NMR spectroscopy (1D, 2D) as well as high-resolution mass spectrometry (Figure S1-S20).

Based on the DFT (B3LYP/6-31G(d)) calculations, the dihedral angles of different helicene substructures were examined. Among them, the dihedral angle of thieno[4]helicene in **1** (Scheme 2, yellow) was predicted to be ~16.7°, which is smaller than that of the pristine carbon analogue [4]helicene (~37°)[16] due to the reduced steric interactions by the introduction of thiophene rings. Likewise, **2** and **3** were estimated to have similar angles of 18.6° and 15.0° at the same cove position. The dihedral angle of thieno[5]helicenes in **2** (Scheme 2, green) was calculated to be 33.4°, which is similar with that of carbo[5]helicenes in **3** (Scheme 2, blue). The carbo[4]helicenes in **2** (Scheme 2, orange) showed the dihedral angle of 24.1°, smaller than that of the carbon analogue [4]helicene (~37°), which is probably affected by the adjacent thieno[4]helicenes. Thanks to the multiple helicene substructures and the corresponding curvatures, compounds **1**-**3** have good solubility in common organic solvents, such as DCM, THF, toluene, etc.

The existence of different helicene substructures results in multiple chirality centers and thus a variety of possible isomers for **1**-**3**. While different atropisomers were observed for precursors **6** and **7** (for rates and energies see SI, chapter 4), the ^{1}H-NMR spectra of **1** and **3** showed well-resolved signals at room temperature (Figure 2, Figure S4 and S14). For **1**, a residual line broadening disappears at slightly increased temperature (Figure S5), which is attributed to the inversion of thieno[4]helicenes. The additional ring fusion of the thienyl moiety results in flattened thieno[4]helicenes in **3** compared to **1** (15.0° vs 16.7°, Scheme 2). Therefore, a faster interconversion is expected, which results in the observed narrow signals for **3** in the temperature range from 30 to 120°C (Figure S20). Compound **2** combines six subhelicenes with three different types of helicene substructures. The ^{1}H-NMR spectrum of **2** is clearly influenced by the dynamic processes (Figure 2b), which were observed over the whole temperature range studies (-30°C–120°C, Figure S11). It can be assumed that the additional carbo[4]helicenes (with a dihedral angle of 24.1°) are the

SCHEME 2. Schematic illustration of the synthesis of NGs 1, 2 and 3. The dihedral angles were calculated at the B3LYP/6-31G(d) level.

Final edited form was published in "Organic Letters". 2021, 23 (6), S. 2069–2073. ISSN 1523-7052.
https://doi.org/10.1021/acs.orglett.1c00232

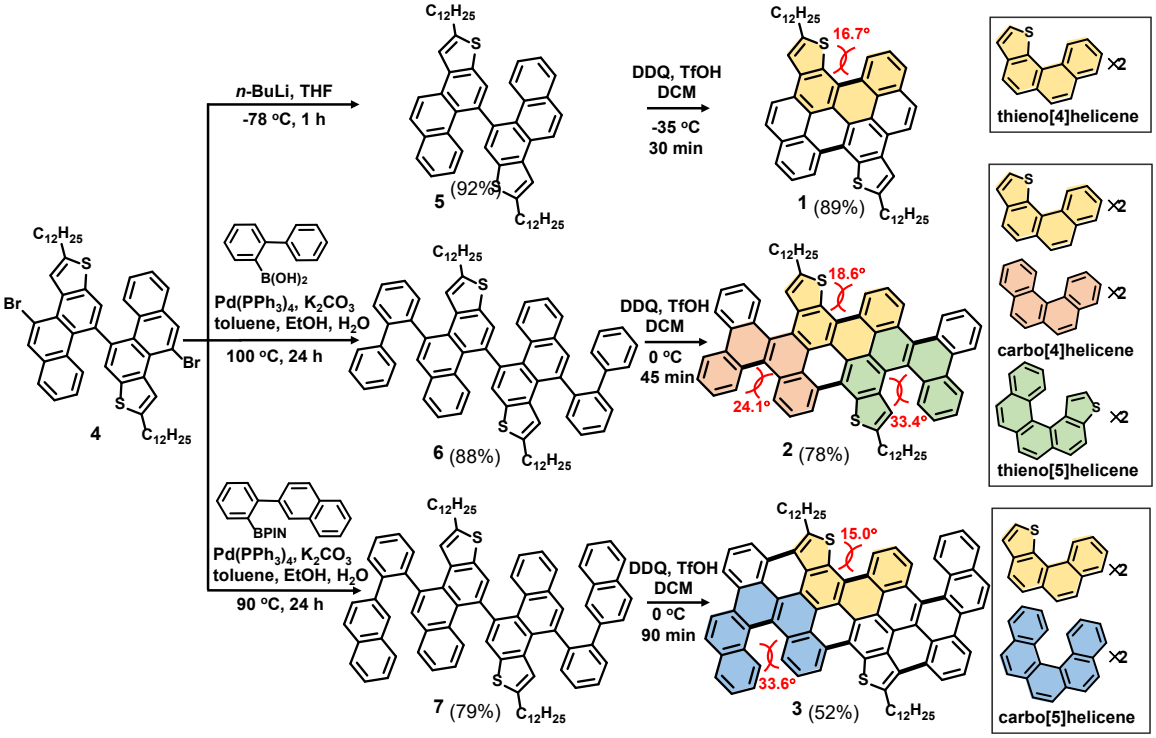

main cause of the line broadening in the NMR spectra of **2**, which is also supported by the broadened signals of H_{24} and H_{25} (Figure 2b). The effect is most pronounced for H_8-H_{10}, which are involved both in the carbo[4]helicene and thieno[4]helicene motions. Fixed helicity of the thieno[5]helicenes in **2** is indicated by signals of two isomers for H_{16} with almost constant ratio and rather narrow signals for H_{16}-H_{19}, which narrow further with increasing temperature (Figure S11). The complex overall dynamic processes of **2** stands for its multi-level helicene substructures in which all individual motions seem to interlock[30].

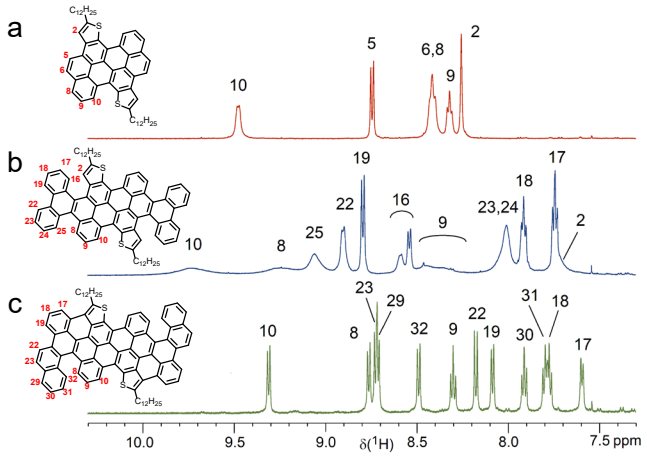

FIGURE 2. ^{1}H-NMR spectra (aromatic region) of **1** (a), **2** (b) and **3** (c) in dichloromethane-d_2 at 30 °C.

The UV-vis absorption spectra of **1**, **2** and **3** in anhydrous DCM solution are presented in Figure 3a. The spectrum of **1** exhibited a maximum absorption peak (λ_{max}) at 449 nm and an absorption onset at 465 nm, corresponding to an optical energy gap of 2.67 eV. In comparison with the reported pristine carbon analogue of **1** (**A**, Figure 1a)[16], which showed a maximum absorption of 502 nm and an optical energy gap of 2.36 eV, the sulfur-doped **1** exhibited an enlarged energy gap. The similar tendency was also found for both **2** and **3** based on the calculation results (Figure S41), compared with their respective carbon analogues. Due to the extended π-conjugation, both **2** and **3** displayed obvious red-shifted absorption peaks compared to **1**, with λ_{max} of 485 and 500 nm. The optical energy gaps of **2** and **3** are estimated to be 2.45 and 2.30 eV, respectively. Compounds **1**-**3** exhibited blue, green, and orange fluorescence, respectively, and their maximum emission peaks were observed at 460, 505 and 569 nm (Figure 3a, dashed line). Interestingly, compound **2** containing three-types of subhelicenes exhibited an absolute quantum yield of 13.8%, higher than those of 4.5% for **1** and 3.8% for **3**. The electrochemical behaviors of **1**-**3** were investigated by cyclic voltammetry (CV) in anhydrous DCM. As illustrated in Figure 3b, compound **1** featured one reversible oxidation wave with half-wave potentials $E^{ox}_{1/2}$ = 0.56 V (vs. Fc^+/Fc), and did not show any reduction process in the cathodic potential range. However, compound **2** displayed two reversible oxidation waves with $E^{ox}_{1/2}$ at 0.47 and 0.89 V, and one reversible reduction wave with $E^{red}_{1/2}$ at -1.96 V. In addition, **3** exhibited two reversible oxidation waves with $E^{ox}_{1/2}$ at 0.42 and 0.91 V, and one reversible reduction wave with $E^{red}_{1/2}$ at -1.88 V. Accordingly, the highest occupied molecular orbital (HOMO)/lowest unoccupied molecular orbital (LUMO) levels were estimated to be -5.29 eV, -5.16/-2.93 eV, and -5.15/-3.03 eV for **1**, **2**, and **3**, respectively, based on the onset potentials of the first oxidation/reduction waves. The electrochemical energy gaps ($E_{g,\,CV}$) were thus calculated to be 2.23 and 2.12 eV for **2** and **3**, respectively, which are in good accordance with their optical energy gaps.

Final edited form was published in "Organic Letters". 2021, 23 (6), S. 2069–2073. ISSN 1523-7052.
https://doi.org/10.1021/acs.orglett.1c00232

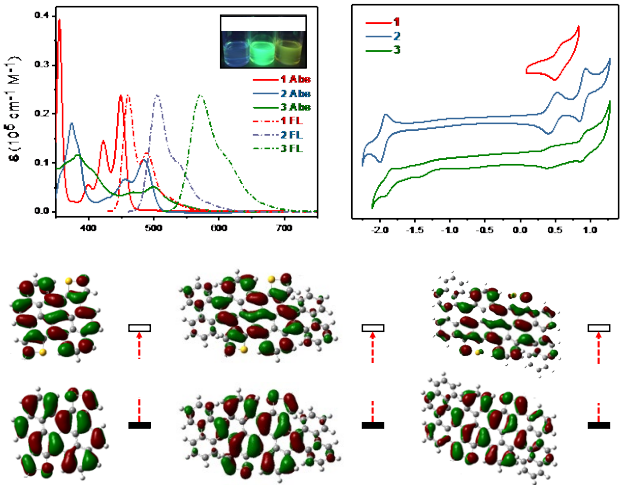

FIGURE 3. (a) UV-vis absorption spectra (solid line) and fluorescence spectra (dashed line) of **1**-**3** in DCM (10^{-5}M). Inset shows the photograph of **1**-**3** under emission. (b) Cyclic voltammograms of **1**-**3** in DCM containing 0.1 M *n*-Bu_4NPF_6 at a scan rate of 0.1 Vs^{-1}. Ferrocene was used as an external standard. (c) Molecular orbitals and their energy diagrams calculated at the B3LYP/6-31G(d) level of **1**-**3**, respectively. Values in brackets represent the oscillator strengths (*f*). H: HOMO; L: LUMO.

To gain deeper insight into their electronic structures, DFT calculations at the B3LYP/6-31G(d) level were performed (Figure 3c). For **1**, both the HOMO and LUMO were delocalized over the entire conjugated backbone. The π-extension of **2** and **3** leads to an enlarged electron delocalization over the whole molecular skeleton. The calculated HOMO and LOMO energy levels as well as energy gaps are summarized in Table S1. Moreover, according to the time-dependent (TD)-DFT calculations, the maximum absorption peaks of **1** (calculated value: 460 nm), **2** (calculated value: 510 nm) and **3** (calculated value: 541 nm) are assignable to the HOMO → LUMO transition, which are in good agreement with the experimentally measured results (Table S1).

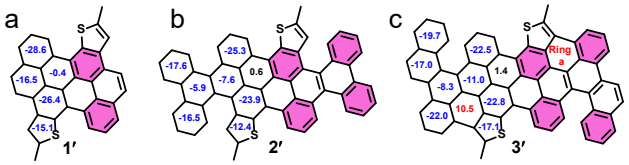

FIGURE 4. NICS(1)$_{zz}$ values (in ppm) of compounds **1′** (a), **2′** (b) and **3′** (c) calculated at the GIAO-B3LYP/6-311+G(2d,p) level.

The nucleus-independent chemical shift (NICS) calculations (Figure 4) were conducted to evaluate the aromaticity of compounds **1**-**3**. The dodecyl groups in **1**-**3** were replaced with methyl groups to simplify the calculations (namely **1′**, **2′**, and **3′**). The NICS(1)$_{zz}$ values of most of rings in **1′**-**3′** are negative, showing the aromatic character. On the contrary, ring a in **3′** shows a positive NICS (1)$_{zz}$ value of 10.5, indicating its anti-aromatic character. According to the NICS calculations, compounds **1**-**3** exhibit aromatic character, in line with their resonance structures (Figure 4, highlighted with pink).

In summary, we demonstrated the novel synthesis of a series of sulfur-doped NGs with multiple helicene substructures. DFT calculations revealed that the subhelicenes in these NGs possess the dihedral angels from 15° to 34°. Compared to the pristine carbon analogues, sulfur-doped NGs showed enlarged energy gaps. These novel sulfur-doped curved NGs hold promise in the applications of optoelectronic devices, and the synthetic strategy described herein can be further extended to synthesize structurally well-defined sulfur-doped graphene nanoribbons.

ASSOCIATED CONTENT

Supporting Information

Experimental details, supporting figures and calculations (PDF).

AUTHOR INFORMATION

Corresponding Author

* mai@sjtu.edu.cn (Y. M.)
Yiyong Mai − School of Chemistry and Chemical Engineering, Frontiers Science Center for Transformative Molecules, Shanghai Key Laboratory of Electrical Insulation and Thermal Ageing, Shanghai Jiao Tong University, Shanghai 200240, China
* juliu@hku.hk (J. L.)
Junzhi Liu − Department of Chemistry and State Key Laboratory of Synthetic Chemistry, The University of Hong Kong, Hong Kong 999077, China

Authors

Wenhui Niu − School of Chemistry and Chemical Engineering, Frontiers Science Center for Transformative Molecules, Shanghai Key Laboratory of Electrical Insulation and Thermal Ageing, Shanghai Jiao Tong University, Shanghai 200240, China; Center for Advancing Electronics Dresden (cfaed) and Faculty of Chemistry and Food Chemistry, Technische Universitat Dresden, D-01062 Dresden, Germany
Yubin Fu − Center for Advancing Electronics Dresden (cfaed) and Faculty of Chemistry and Food Chemistry, Technische Universitat Dresden, D-01062 Dresden, Germany
Hartmut Komber − Leibniz-Institut für Polymerforschung Dresden e.V., D-01069 Dresden, Germany
Ji Ma − Center for Advancing Electronics Dresden (cfaed) and Faculty of Chemistry and Food Chemistry, Technische Universitat Dresden, D-01062 Dresden, Germany
Xinliang Feng − Center for Advancing Electronics Dresden (cfaed) and Faculty of Chemistry and Food Chemistry, Technische Universitat Dresden, D-01062 Dresden, Germany

Author Contributions

The manuscript was written through contributions of all authors.

Notes

The authors declare no competing financial interest.

ACKNOWLEDGMENT

Y. M. is grateful for the financial support from the National Natural Science Foundation of China (21774076 and 52073173), the Program of Shanghai Academic Research Leader (19XD1421700) and the Program of Distinguished Professor of Special Appointment at Shanghai Institutions of Higher Learning. X. F. thanks the European Union's Horizon 2020 (No 881603 Graphene Flagship Core3, No 813036 Marie Skłodowska-Curie), ERC Grant on T2DCP, German DFG (Cluster of Excellence "Center for Advancing Electronics Dresden (cfaed)" and DFG NSFC Joint Sino-German Research Project (EnhanceNano), as well as the DFG-SNSF Joint Switzerland-German Research Project (EnhanTopo). J. L. is grateful for the Hong Kong Research Grants Council (HKU 27301720) and the funding support from ITC to the SKL. We are grateful for the assistance of F. Drescher and Prof. E. Brunner for the HR-MS measurements. We also appreciate the Instrumental Analysis Center at Shanghai Jiao Tong University for some analyses. We thank the Center for Information Services and High Performance Computing

Final edited form was published in "Organic Letters". 2021, 23 (6), S. 2069–2073. ISSN 1523-7052.
https://doi.org/10.1021/acs.orglett.1c00232

(ZIH) at TU Dresden for generous allocations of compute resources.

REFERENCES

(1) Pun, S. H.; Miao, Q., Toward Negatively Curved Carbons. *Acc. Chem. Res.* **2018**, *51*, 1630-1642.
(2) Kawasumi, K.; Zhang, Q.; Segawa, Y.; Scott, L. T.; Itami, K., A grossly warped nanographene and the consequences of multiple odd-membered-ring defects. *Nat. Chem.* **2013**, *5*, 739-744.
(3) Ball, M.; Zhong, Y.; Wu, Y.; Schenck, C.; Ng, F.; Steigerwald, M.; Xiao, S.; Nuckolls, C., Contorted Polycyclic Aromatics. *Acc. Chem. Res.* **2015**, *48*, 267-276.
(4) Zhu, Y.; Xia, Z.; Cai, Z.; Yuan, Z.; Jiang, N.; Li, T.; Wang, Y.; Guo, X.; Li, Z.; Ma, S.; Zhong, D.; Li, Y.; Wang, J., Synthesis and Characterization of Hexapole [7]Helicene, A Circularly Twisted Chiral Nanographene. *J. Am. Chem. Soc.* **2018**, *140*, 4222-4226.
(5) Wang, Y.; Yin, Z.; Zhu, Y.; Gu, J.; Li, Y.; Wang, J., Hexapole [9]Helicene. *Angew. Chem. Int. Ed.* **2019**, *58*, 587-591.
(6) Fernández-García, J. M.; Evans, P. J.; Filippone, S.; Herranz, M. Á.; Martín, N., Chiral Molecular Carbon Nanostructures. *Acc. Chem. Res.* **2019**, *52*, 1565-1574.
(7) Naaman, R.; Waldeck, D. H., Chiral-Induced Spin Selectivity Effect. *J. Phys. Chem. Lett.* **2012**, *3*, 2178-2187.
(8) Gingras, M., One hundred years of helicene chemistry. Part 3: applications and properties of carbohelicenes. *Chem. Soc. Rev.* **2013**, *42*, 1051-1095.
(9) Rickhaus, M.; Mayor, M.; Juríček, M., Strain-induced helical chirality in polyaromatic systems. *Chem. Soc. Rev.* **2016**, *45*, 1542-1556.
(10) Shen, Y.; Chen, C.-F., Helicenes: Synthesis and Applications. *Chem. Rev.* **2012**, *112*, 1463-1535.
(11) Ogawa, N.; Yamaoka, Y.; Takikawa, H.; Yamada, K.-i.; Takasu, K., Helical Nanographenes Embedded with Contiguous Azulene Units. *J. Am. Chem. Soc.* **2020**, *142*, 13322-13327.
(12) Ma, J.; Fu, Y.; Dmitrieva, E.; Liu, F.; Komber, H.; Hennersdorf, F.; Popov, A. A.; Weigand, J. J.; Liu, J.; Feng, X., Helical Nanographenes Containing an Azulene Unit: Synthesis, Crystal Structures, and Properties. *Angew. Chem. Int. Ed.* **2020**, *59*, 5637-5642.
(13) Nakakuki, Y.; Hirose, T.; Sotome, H.; Miyasaka, H.; Matsuda, K., Hexa-peri-hexabenzo[7]helicene: Homogeneously π-Extended Helicene as a Primary Substructure of Helically Twisted Chiral Graphenes. *J. Am. Chem. Soc.* **2018**, *140*, 4317-4326.
(14) Fujikawa, T.; Preda, D. V.; Segawa, Y.; Itami, K.; Scott, L. T., Corannulene–Helicene Hybrids: Chiral π-Systems Comprising Both Bowl and Helical Motifs. *Org. Lett.* **2016**, *18*, 3992-3995.
(15) Fernández-García, J. M.; Evans, P. J.; Medina Rivero, S.; Fernández, I.; García-Fresnadillo, D.; Perles, J.; Casado, J.; Martín, N., π-Extended Corannulene-Based Nanographenes: Selective Formation of Negative Curvature. *J. Am. Chem. Soc.* **2018**, *140*, 17188-17196.
(16) Liu, J.; Li, B.-W.; Tan, Y.-Z.; Giannakopoulos, A.; Sanchez-Sanchez, C.; Beljonne, D.; Ruffieux, P.; Fasel, R.; Feng, X.; Müllen, K., Toward Cove-Edged Low Band Gap Graphene Nanoribbons. *J. Am. Chem. Soc.* **2015**, *137*, 6097-6103.
(17) Kashihara, H.; Asada, T.; Kamikawa, K., Synthesis of a Double Helicene by a Palladium-Catalyzed Cross-Coupling Reaction: Structure and Physical Properties. *Chem. Eur. J.* **2015**, *21*, 6523-6527.
(18) Zhang, F.; Michail, E.; Saal, F.; Krause, A.-M.; Ravat, P., Stereospecific Synthesis and Photophysical Properties of Propeller-Shaped $C_{90}H_{48}$ PAH. *Chem. Eur. J.* **2019**, *25*, 16241-16245.
(19) Li, C.; Yang, Y.; Miao, Q., Recent Progress in Chemistry of Multiple Helicenes. *Chem. Asian J.* **2018**, *13*, 884-894.
(20) Mori, T., Chiroptical Properties of Symmetric Double, Triple, and Multiple Helicenes. *Chem. Rev.* **2021**.
(21) Wang, X.-Y.; Yao, X.; Narita, A.; Müllen, K., Heteroatom-Doped Nanographenes with Structural Precision. *Acc. Chem. Res.* **2019**, *52*, 2491-2505.
(22) Narita, A.; Wang, X.-Y.; Feng, X.; Müllen, K., New advances in nanographene chemistry. *Chem. Soc. Rev.* **2015**, *44*, 6616-6643.
(23) Liu, J.; Feng, X., Bottom-Up Synthesis of Nitrogen-Doped Polycyclic Aromatic Hydrocarbons. *Synlett* **2020**, *31*, 211-222.
(24) Stępień, M.; Gońka, E.; Żyła, M.; Sprutta, N., Heterocyclic Nanographenes and Other Polycyclic Heteroaromatic Compounds: Synthetic Routes, Properties, and Applications. *Chem. Rev.* **2017**, *117*, 3479-3716.
(25) Xu, K.; Fu, Y.; Zhou, Y.; Hennersdorf, F.; Machata, P.; Vincon, I.; Weigand, J. J.; Popov, A. A.; Berger, R.; Feng, X., Cationic Nitrogen-Doped Helical Nanographenes. *Angew. Chem. Int. Ed.* **2017**, *56*, 15876-15881.
(26) Chen, L.; Mali, K. S.; Puniredd, S. R.; Baumgarten, M.; Parvez, K.; Pisula, W.; De Feyter, S.; Müllen, K., Assembly and Fiber Formation of a Gemini-Type Hexathienocoronene Amphiphile for Electrical Conduction. *J. Am. Chem. Soc.* **2013**, *135*, 13531-13537.
(27) Chen, L.; Puniredd, S. R.; Tan, Y.-Z.; Baumgarten, M.; Zschieschang, U.; Enkelmann, V.; Pisula, W.; Feng, X.; Klauk, H.; Müllen, K., Hexathienocoronenes: Synthesis and Self-Organization. *J. Am. Chem. Soc.* **2012**, *134*, 17869-17872.
(28) Chiu, C.-Y.; Kim, B.; Gorodetsky, A. A.; Sattler, W.; Wei, S.; Sattler, A.; Steigerwald, M.; Nuckolls, C., Shape-shifting in contorted dibenzotetrathienocoronenes. *Chem. Sci.* **2011**, *2*, 1480-1486.
(29) Fujikawa, T.; Segawa, Y.; Itami, K., Synthesis and Structural Features of Quadruple Helicenes: Highly Distorted π Systems Enabled by Accumulation of Helical Repulsions. *J. Am. Chem. Soc.* **2016**, *138*, 3587-3595.
(30) Hosokawa, T.; Takahashi, Y.; Matsushima, T.; Watanabe, S.; Kikkawa, S.; Azumaya, I.; Tsurusaki, A.; Kamikawa, K., Synthesis, Structures, and Properties of Hexapole Helicenes: Assembling Six [5]Helicene Substructures into Highly Twisted Aromatic Systems. *J. Am. Chem. Soc.* **2017**, *139*, 18512-18521.